

Polar molecule reactive collisions in quasi-1D systems

A. Simoni^a, S. Srinivasan^a, J-M. Launay^a, K. Jachymski^b, Z. Idziaszek^b, and P. S. Julienne^c

^aInstitut de Physique de Rennes, UMR 6251 du CNRS and Université de Rennes 1, 35042 Rennes Cedex, France

^b Faculty of Physics, University of Warsaw, Pasteura 5, 02-093 Warsaw, Poland

^c Joint Quantum Institute, University of Maryland and National Institute of Standards and Technology, College Park, Maryland 20742, USA

Abstract. We study polar molecule scattering in quasi-one-dimensional geometries. Elastic and reactive collision rates are computed as a function of collision energy and electric dipole moment for different confinement strengths. The numerical results are interpreted in terms of first order scattering and of adiabatic models. Universal dipolar scattering is also discussed. Our results are relevant to experiments where control of the collision dynamics through one dimensional confinement and an applied electric field is envisioned.

PACS numbers: 34.50.-s, 31.15.-p

Introduction

Ultracold gases of polar molecules generate considerable theoretical and experimental interest (Quemener & Julienne 2012). Systems composed of polar molecules in optical lattices are expected to give rise to a variety of novel quantum phases (Góral et al. 2002, Yi et al. 2007, Sinha & Santos 2007, Capogrosso-Sansone et al. 2010, Wall & Carr 2010, Gorshkov et al. 2011, Sowiński et al. 2012). The presence of dipolar confinement-induced resonances has been theoretically addressed for nonreactive molecules in reduced quasi-1D geometries (Giannakeas et al. 2013, Bartolo et al. 2013). Understanding reactive processes is also relevant in quantum chemistry at extremely low temperature (Krems 2008, Carr et al. 2009). For instance, in three dimensions a fast chemical rate between ultracold fermionic K-Rb molecules has been found (Ospelkaus et al. 2010), which rapidly increases even further if the molecules are polarized by an external electric field (Ni et al. 2010). These results have been theoretically explained based on effective two-body quantum reaction models (Quémener & Bohn 2010*b*, Idziaszek & Julienne 2010).

Unfortunately, at least for reactive species, reaction events are usually responsible for a short lifetime of the trapped molecular sample which may impair the observation of interesting collective phenomena. In order to overcome this limitation, scattering of reactive molecules in two-dimensional pancake shaped traps has been experimentally studied in (de Miranda et al. 2011). In this geometry, the repulsion between molecules with dipoles parallel to the trap axis allows the reactive rate constants to be suppressed, as confirmed by quantum theoretical calculations (Quémener & Bohn 2010*a*, Micheli et al. 2010).

Recent experimental work addressing fermionic K-Rb molecules in quasi-1D systems shows that reactive processes are very sensitive to both the intensity of polarizing electric fields and to the depth of an additional lattice along the system axis (Chotia et al. 2012). However, the amount of data concerning the influence of the electric field on the scattering dynamics reported in (Chotia et al. 2012) is relatively limited. Motivated by ongoing experimental studies on ultracold K-Rb and other rapidly developing experiments with ultracold molecules, in the present work we address theoretically scattering of reactive polar molecules in quasi 1D geometry achieved by tight lattice confinement in two directions at very low collision energy for a variety of trapping and molecular interaction parameters. We focus on the cases of identical fermions or bosons, which are both achievable experimentally. We discuss emergence of universal scattering in 1D configurations for strong dipole moments. As we restrict our considerations to a two-body scattering problem, we will not take into account the many-body correlations which can have strong impact on the dissipative dynamics of quasi-one-dimensional gases (Syassen et al. 2008, Zhu et al. 2014).

The paper is organized as follows. We first present the theoretical model and our computational approach. We then summarize and discuss our results for different confinement strengths as a function of collision energy, dipole moment and orientation.

When possible we interpret the results based on analytical or effective models. A short conclusion ends this work.

1. Model

The short range dynamics of a molecule-molecule collision is a complex reactive four-body problem very difficult to treat theoretically, in particular in the ultracold regime. In this work we follow the approach of (Micheli et al. 2010) by limiting ourselves to an asymptotic model where the collision process is described as an effective two-body problem at intermolecular distances larger than a_c which denotes the distance where atom exchange processes take place. Then the reaction phenomena can simply be taken into account by introducing a WKB-like boundary condition that guarantees a given fraction of the flux reaching the short range $r \sim a_c$ to give rise to reaction (Micheli et al. 2010). Such fraction is an empirical parameter in the model and will be taken to be unity (total absorption) in the present work as suggested by experiments performed on fermionic K-Rb molecules (Ospelkaus et al. 2010). This approach corresponds to the so-called universal regime where short range interaction details do not influence the dynamics. The model can easily be generalized to nonuniversal cases as well (Idziaszek & Julienne 2010, Jachymski et al. 2013).

The presence of external fields induce an effective dipole moment in the molecules, which we will treat as fixed along the field axis. After separation of the center of mass, the potential for two fixed dipoles $\vec{d} = d\hat{n}$ oriented along the \hat{n} direction and subject to 2D harmonic confinement with frequency ν_\perp reads

$$H = -\frac{\hbar^2}{2\mu}\Delta + \frac{1}{2}\mu\omega_\perp^2\rho^2 + V_{int}(\vec{r}), \quad (1)$$

with ρ the distance to the trap axis z and $\omega_\perp = 2\pi\nu_\perp$ the angular oscillation frequency. In the outer region of radial distances $r > a_c$ the intermolecular interaction V_{int} takes a simple form comprising to leading order the isotropic van der Waals interaction and the anisotropic potential between oriented dipoles $\vec{d} = d\hat{n}$

$$V_{int}(\vec{r}) = V_{vdW} + V_{dd} = -\frac{C_6}{r^6} + \frac{d^2}{r^3} [1 - 3(\hat{n} \cdot \hat{r})^2]. \quad (2)$$

We ignore in this work the correlated fluctuations of molecular dipoles at short range which can become important and give rise to resonant effects as the molecular dipole increases (Julienne et al. 2011). Within the present model, the importance of the different terms in the Hamiltonian can be summarized in typical natural lengthscales. The average scattering length for a van der Waals potential $\bar{a} = 2\pi/\Gamma^2(1/4)(2\mu C_6/\hbar^2)^{1/4}$ first introduced in (Gribakin & Flambaum 1993), the dipolar length $a_{dd} = \mu d^2/\hbar^2$, and the harmonic oscillator length $a_{ho} = \sqrt{\hbar/\mu\omega_\perp}$ will be used respectively to estimate the range of the isotropic, anisotropic dipolar, and of the harmonic confinement potentials. Sample values of the trapping and molecular parameters are reported for reference in table 1 for reactive molecules with a mild (K-Rb) and strong (Li-Cs) proper dipole moment.

Table 1. Characteristic trapping and potential parameters as defined in the text for two sample reactive polar molecules with relatively small (K-Rb) and large (Li-Cs) electric dipole moment. Three sets of parameters corresponding to the weak, intermediate and strong confinement cases discussed in the text are provided. Two specific values of electric dipole d_1 and d_2 at which $a_{\text{dd}} = \bar{a}$ and $a_{\text{dd}} = a_{ho}$ are also given for reference. Van der Waals coefficients are from (Kotochigova 2010) and (Żuchowski et al. 2013) for K-Rb and Li-Cs, respectively. Note that for the sake of completeness values larger than the permanent K-Rb dipole moment of 0.57 D have also been used in the calculations.

System	$\bar{a}(a_0)$	$a_{ho}(a_0)$	$\nu_{\perp}(\text{MHz})$	$\hbar\omega_{\perp}/k_B(\mu\text{K})$	$d_1(\text{D})$	$d_2(\text{D})$
K-Rb	118	1.18×10^4	4.08×10^{-4}	1.96×10^{-2}	8.12×10^{-2}	8.12×10^{-1}
		1.18×10^3	4.08×10^{-2}	1.96		2.57×10^{-1}
		1.18×10^2	4.08	1.96×10^2		8.12×10^{-2}
Li-Cs	256	2.56×10^4	8.24×10^{-4}	3.95×10^{-2}	3.69×10^{-1}	3.69
		2.56×10^3	8.24×10^{-2}	3.95		1.17
		2.56×10^2	8.24	3.95×10^2		3.69×10^{-1}

The collision process will be described in terms of the scattering matrix elements $S_{j'j}$ between the eigenstates $|j\rangle = |n_r\Lambda\rangle$ of the transverse quantum oscillator in the ρ direction with radial quantum number $n_r = 0, 1, \dots$, axial angular momentum Λ , and energy $E_{n_r\Lambda} = \hbar\omega_{\perp}(2n_r + |\Lambda| + 1)$. The asymptotic scattering wavefunction for bosonic and fermionic exchange symmetry can be expressed in terms of ingoing and outgoing waves along the trap axis as

$$\Psi^{(j)\text{B,F}}(r) \sim q_j^{-1/2} e^{-iq_j|z|} |j\rangle \pm \sum_{j'} q_{j'}^{-1/2} e^{iq_{j'}|z|} S_{j'j}^{\text{B,F}} |j'\rangle \quad , \quad r \rightarrow \infty \quad (3)$$

where $q_j = \sqrt{2\mu(E - E_j)}/\hbar$ is the wavevector in channel j . The upper (lower) sign holding for bosons (fermions) in (3) guarantees that in the absence of interaction $S_{j'j} = \delta_{j'j}$. Finally, the inelastic state-to-state collision rate $\mathcal{K}_{j'j}$ for $|j\rangle \rightarrow |j'\rangle$ transitions is expressed in terms of the S matrix elements as $\mathcal{K}_{j'j}^{\text{B,F}} = v_j \left| \delta_{j'j} - S_{j'j}^{\text{B,F}} \right|^2$, with $v_j = \hbar q_j / \mu$ the relative velocity in channel j .

1.1. Wigner laws and Born approximation

The effective potential between polar molecules has a long-range inverse-cube character that profoundly modifies the usual Wigner laws valid for short range potentials (Sadeghpour et al. 2000). The corresponding asymptotic low energy expansion of the elastic phase shift has been derived in (Gao 1999, Muller 2013) for isotropic repulsive and attractive inverse cube potentials, respectively. In order to generalize these results to the case of a complex boundary condition, we first define a complex phase shift for bosons and fermions as $\tan(\delta^{\text{B,F}}) = i(1 - S_{jj}^{\text{B,F}})/(1 + S_{jj}^{\text{B,F}})$ (Micheli

et al. 2010), where the channel index j on the lhs has been, and will henceforth be unless needed, left implicit for notational convenience. We can then express the phase shift as

$$\tan(\delta^F) = -(qb_3) \log(|b_3|q) - q(\alpha^F - i\beta^F) \quad (4)$$

and

$$\tan(\delta^B) = \frac{1}{(qb_3) \log(|b_3|q) + q(\alpha^B - i\beta^B)} \quad (5)$$

in terms of an algebraic length $b_3 = 2a_{\text{dd}} [3(\hat{n} \cdot \hat{z})^2 - 1]$ that characterizes the strength of the dipolar interaction for oriented molecules. This definition corresponds to an asymptotically attractive (repulsive) dipolar interaction $-b_3/z^3$ for $b_3 > 0$ ($b_3 < 0$).

The leading order $q \log(|b_3|q)$ is universal in that it only depends on the long-range dipolar interaction. Its value can also be obtained in the Born approximation which can be shown to be exact in the zero energy limit for long range potentials (Delves 1960). The next order energy correction is proportional to the complex length $(\alpha - i\beta)$ which, in addition to \vec{d} , also depends on the details of the short-range dynamics, with the imaginary part β accounting in particular for inelastic and reactive processes. We will often term in the following α and β the elastic and inelastic collision lengths, respectively.

As the dipolar force becomes dominating the purely dipolar model (Muller 2013) shows that for $b_3 > 0$ the scaling of α and β is set by a_{dd} . Similarly, in the $b_3 < 0$ regime according to (Gao 1999) one may expect $\alpha \sim a_{\text{dd}}$. However, we anticipate that since for $b_3 < 0$ the dipolar repulsive potential creates a barrier to the reaction, depending on collision energy and on the confinement strength the inelastic length β may not scale with a_{dd} and can be exponentially suppressed.

If $(\alpha - i\beta)$ is considered to be a momentum-dependent quantity (finite for $q \rightarrow 0$) the parametrizations (4) and (5) are indeed exact. The corresponding elastic scattering rates can be expressed using the general formulas in (Naidon & Julienne 2006) as

$$\mathcal{K}^{\text{el},B} \equiv \mathcal{K}_{jj}^B = \frac{4\hbar q}{\mu} \frac{1}{q^2 [\alpha^B + b_3 \log(|b_3|q)]^2 + (1 + q\beta^B)^2} \quad (6)$$

and

$$\mathcal{K}^{\text{el},F} \equiv \mathcal{K}_{jj}^F = \frac{4\hbar q^3}{\mu} \frac{[\alpha^F + b_3 \log(|b_3|q)]^2 + (\beta^F)^2}{q^2 [\alpha^F + b_3 \log(|b_3|q)]^2 + (1 + q\beta^F)^2} \quad (7)$$

for bosons and fermions, respectively. The total inelastic plus reactive rate from channel j takes the form

$$\mathcal{K}^{\text{inel}} = v_j(1 - |S_{jj}^{B,F}|^2) = \frac{4\hbar q^2}{\mu} \frac{\beta^{B,F}}{q^2 [\alpha^{B,F} + b_3 \log(|b_3|q)]^2 + (1 + q\beta^{B,F})^2} \quad (8)$$

for bosons and fermions alike. The purely reactive rate for molecules in channel j is finally expressed through the lack of unitarity of the S matrix as $\mathcal{K}^{\text{react}} = v_j(1 - \sum_{j'} |S_{j'j}|^2)$. In striking contrast with the 3D case, for bosons in one dimension the elastic scattering rate will dominate the reactive rate if the collision energy is sufficiently small. The effect of the full potential at collision energy E can also be conveniently

summarized in a complex one dimensional scattering length (Olshanii 1998, Bolda et al. 2002), defined as

$$a_{1D}^B(q) = \lim_{q \rightarrow 0} \frac{1}{q \tan(\delta^B)} \quad , \quad a_{1D}^F(q) = -\lim_{q \rightarrow 0} \frac{\tan(\delta^F)}{q}. \quad (9)$$

Using eqs. (4) and (5) one promptly obtains

$$a_{1D}^{B,F}(q) = b_3 \log(|b_3|q) + \alpha^{B,F} - i\beta^{B,F}. \quad (10)$$

In order to clarify the rationale for the different conventions adopted so far, we remark that for purely elastic scattering in a short-range potential the zero-energy wave function will take at long range the familiar form $\Psi \sim (|z| - a_{1D})$ for both bosons and fermions. Note however that if $d \neq 0$, the logarithmic singularity in eq. (10) makes a_{1D} an intrinsically energy-dependent quantity that does not admit a finite zero-energy limit. It will be shown in the following that such Wigner laws set in at energies well below the typical current experimental conditions and may not be directly observable.

In 3D, elastic collisions in the presence of dipole-dipole interactions are well described using Born approximation. Similar approach has been already applied in quasi-2D geometry as well (Micheli et al. 2010). In the present quasi-one-dimensional case, we will make use of the distorted wave Born approximation (DWBA) for interpretation purposes.

In this method we first calculate the scattering amplitude and the wave function for van der Waals interaction alone using standard Born approximation and then include the dipole-dipole interactions on top of it. The van der Waals scattering amplitudes within our definitions yield

$$f_{\text{vdW}}^B(q) = -\frac{1}{iqa_{1D}^B(q) + 1} \quad , \quad f_{\text{vdW}}^F(q) = \frac{1}{i/(qa_{1D}^F(q)) - 1}, \quad (11)$$

where in the limit of $\bar{a} \ll a_{ho}$ and $q \rightarrow 0$ we have (Micheli et al. 2010)

$$a_{1D}^B(q) \xrightarrow{q \rightarrow 0} -\frac{a_{ho}^2}{4\bar{a}}(1+i) \quad , \quad a_{1D}^F(q) \xrightarrow{q \rightarrow 0} -\frac{6\bar{a}^2\bar{a}_1}{a_{ho}^2}(1+i). \quad (12)$$

Here $\bar{a}_1 = \Gamma(1/4)^6/(144\pi^2\Gamma(3/4)^2)\bar{a} \approx 1.064\bar{a}$ (Idziaszek & Julienne 2010). The total scattering amplitude in DWBA is given as a sum $f = f_{\text{vdW}} + f_{\text{dd}}$, where f_{dd} is now calculated including the phase shift from van der Waals interaction

$$f_{\text{dd}}^{B,F}(q) = -4ie^{2i\delta_{\text{vdW}}^{B,F}(q)} \frac{a_{\text{dd}}}{qa_{ho}} I^{B,F}(q), \quad (13)$$

where

$$I^B(q) = \int_0^\infty d\rho \int_0^\infty dz \cos^2(qz + \delta_{\text{vdW}}^B) e^{-\rho^2} \frac{z^2 - \rho^2/2}{(z^2 + \rho^2)^{5/2}} \quad (14)$$

and for fermions the cos under the integral has to be replaced with sin. This formula assumes that the particles are in the ground state of transverse harmonic oscillator and can easily be generalized by replacing the ground state wave function with an excited one. Finally equations (11) are inverted to obtain from the full scattering amplitude f the energy dependent scattering lengths.

1.2. Numerical calculations

Details on the computational algorithm used for the present problem will be given elsewhere and we limit ourselves here to providing the main elements.

In our approach the scattering equations are written in spherical coordinates and the interaction volume is partitioned in two regions in which the wavefunction is expanded on different basis sets. In the internal region a basis of spherical harmonics $Y_{\ell m}$ is used. In practical calculations we find that numerical convergence is optimal if the small r region is made to extend up to about $10 a_{ho}$. Note that the Hamiltonian (1) is symmetric with respect to reflection about each plane containing the trap axis and about the plane orthogonal to the trap axis and containing the origin. The Hamiltonian matrix can therefore be partitioned into eight noninteracting blocks labeled by $\{\pi_x \pi_y \pi_z\}$, with $\pi_{x,y,z} = \pm 1$ for positive and negative parity, thus leading to significant computational saving. Moreover, according to the tensor order 2 of the intermolecular interaction and trapping potential, only states with $\Delta\ell = 0, \pm 2$ and $\Delta m = 0, \pm 2$ are coupled, resulting in a highly sparse interaction matrix. Identical particle symmetry in the present spinless case is equivalent to total parity $\pi = \pi_x \pi_y \pi_z$ and requires that even (odd) partial waves only are allowed for identical bosons (fermions).

In the external region the cylindrical trapping potential tends to confine the wavefunction to small angular regions near the poles, making the development in spherical harmonics inefficient. In this region we use therefore an adapted primitive basis obtained by projecting cylindrical grid (DVR) functions on the spherical surface. Such basis functions inherently depend on the distance ρ to the trap axis and therefore naturally adapt with varying r to the cylindrical symmetry of the problem. Our grid excludes the pole $\theta = 0$ in order to avoid the singularity of the orbital angular momentum operator $\vec{\ell}^2$ at this point. The boundary condition imposed at the other grid edge is that the wavefunction vanishes at (and beyond) a given distance to the axis ρ_{\max} . Such DVR grid containing only one edge point is known as of Gauss-Lobatto-Radau type.

The radial wavefunction is computed with exponential numerical accuracy up to a distance r_∞ using the spectral element approach we recently adapted to molecular physics. In such approach the radial domain is partitioned in bins and the scattering problem is cast as a linear system for a sparse matrix which is solved using state-of-the-art computer packages. One main advantage of our method is that the extremely sparse nature of the interaction potential is fully taken advantage of.

Note that in the external region we do not work directly in the primitive basis but find it convenient to use a diabatic-by-sector approach in which the Hamiltonian is diagonalized at the center of each bin and the wavefunction is developed (in the given bin) on a small number of the resulting eigenvectors (Lepetit et al. 1986).

Finally, the reactance and hence the scattering matrices are extracted by matching the wavefunction at r_∞ to asymptotic reference functions expressed in cylindrical coordinates. The explicit formulas and procedure are a direct generalization of the ones in (Simoni & Launay 2011) where one must now also sum over different values of

Λ . Moreover, in order to enforce the correct Wigner law for an effective z^{-3} potential it is essential to correct the trigonometric reference functions using first order Born approximation. To this aim a semianalytical procedure based on the evaluation of exponential integrals in the same spirit of (Rawitscher et al. 1999) has been implemented in our algorithm.

2. Results and discussion

In spite of the simplifying assumptions at the basis of our model, the problem is still relatively complex as it depends on the three independent length scales \bar{a} , a_{ho} , and a_{dd} arising from the different interaction terms in the Hamiltonian, on the collision energy E , on the molecular dipole orientation, and on the initial quantum state for the collision. We will present our results according to a classification based on the confinement strength of the trap, that will be referred to as weak, intermediate, and strong, corresponding respectively to $a_{ho} = 10^n \bar{a}$ with $n = 2, 1, 0$. Whereas this

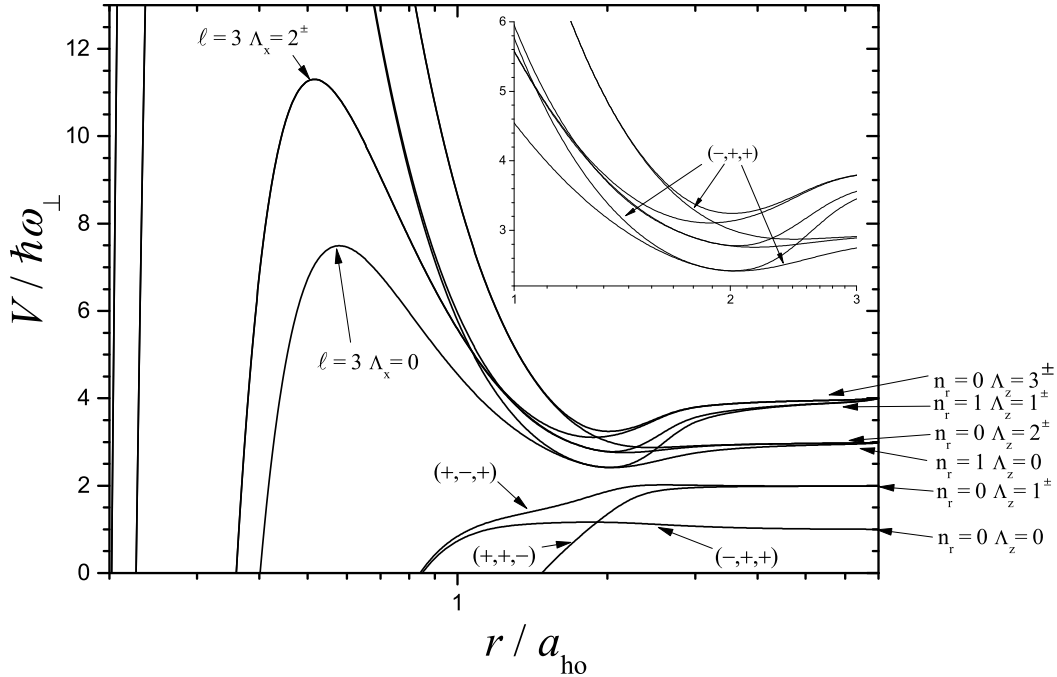


Figure 1. Adiabatic potential curves in spherical coordinates for fermionic K-Rb molecules with $d = 0.5$ D and $\nu_{\perp} = 50$ kHz. The n_r denotes the radial quantum number of 2D harmonic oscillator, Λ_z the projection of the angular momentum on the trap axis and Λ_x on the dipoles axis. We note that Λ_z becomes a good quantum number at large distances, and Λ_x is approximately good only at distances where the trap can be neglected. The \pm signs refer to the reflection symmetry with respect to the sign change of each of the (x, y, z) Cartesian coordinates.

convention denotes the strength of the confinement with respect to the isotropic part

of the potential, one should note from table 1 that for ordinary molecular parameters the dipolar length a_{dd} may easily become the dominant length scale in the problem. We will mainly focus on the case when the orientation of the dipoles is perpendicular to the trap axis, unless stated otherwise. For the sake of a more direct comparison with experiments most of our results will be expressed in dimensional form using K-Rb physical parameters. For completeness, we will however also consider values of d larger than the proper physical dipole moment of K-Rb. Since the model is universal, if needed it is easy to transpose the present data to other polar molecule systems by dimensional scaling.

To interpret our numerical results, we will make use of simpler models. DWBA will be applied to describe the elastic rates. In order to understand the behavior of inelastic rates, one can use the adiabatic approximation. In this method one aims to partially diagonalise the problem. Depending on the chosen coordinate system, one either diagonalises the angular part of the wave function at each distance r or the (ρ, ϕ) dependent part at each distance z . The former choice better reflects the symmetry of the interaction, while the latter is more suited to the trapping potential, but neither will fully cover all the features of the system. Below we use spherical coordinates. The partial diagonalisation results in a set of adiabatic curves $\lambda_n(r)$, which act as an effective potential that can be plugged into radial Schrödinger equation. This method cannot be expected to give strictly quantitative results for the reaction rates, but nicely shows the couplings between different states. Figure 1 shows an exemplary set of adiabatic curves for identical fermions with $d = 0.5$ D confined in a trap with frequency $\nu_{\perp} = 50$ kHz, giving $a_{ho} = 3.6 \bar{a}$, between the medium and strong confinement case. At large distances, when the dipole-dipole interaction becomes negligible, the adiabatic potentials correspond to the states of two-dimensional harmonic oscillator. At smaller r the interplay between the centrifugal barrier and the interaction becomes crucial, which is why spherical coordinates seem to be the better choice here. One can see that strong dipolar interactions can completely remove the barrier for the lowest adiabatic curve. To get an estimate of the rate constant in the energetically lowest channel we then restrict ourselves to the lowest adiabatic curve, imposing MQDT boundary conditions at short range. This neglects the nonadiabatic couplings, but still qualitatively reproduces the full numerical results, as will be shown in the next sections. This is the case because the main factor determining the rates is the height of the adiabatic barrier that has to be overcome by the particles. Adiabatic barrier heights for both bosons and fermions at low and medium confinement are given in figure 2. Obviously, at zero dipole moment the barrier is present only for fermions. For strong dipoles the barrier height becomes independent of the quantum statistics, as the dipole-dipole interaction starts to dominate over the centrifugal barrier.

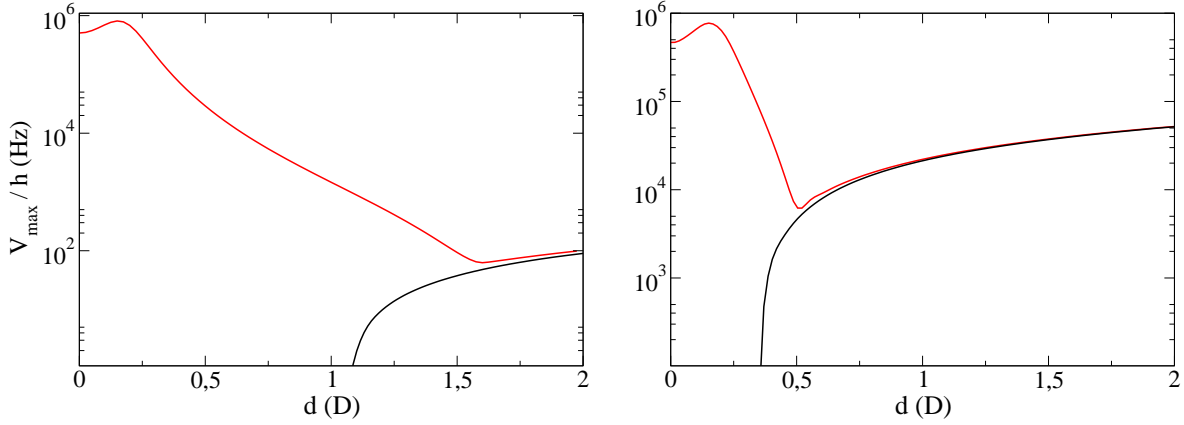


Figure 2. Adiabatic barrier heights for weak (left) and intermediate (right) confinement corresponding to $a_{ho} = 100\bar{a}$ and $10\bar{a}$, respectively, for bosons (black curves) and fermions (red curves). The reduced mass and C_6 of K-Rb molecules is assumed.

2.1. Weak confinement

Let us now consider scattering in a weakly confining trap $a_{ho} = 10^2 \bar{a}$ for molecules in the lowest transverse trap level $|n_r \Lambda\rangle = |00\rangle$. For vanishing d and $E \rightarrow 0$ the scattering problem can be solved essentially exactly relying on the separation of length scales $a_c \ll \bar{a} \ll a_{ho}$ (Michele et al. 2010). Under these conditions motion at short range is unaffected by the trap and is driven by the spherically symmetric van der Waals interaction. Moreover, the low collision energy in the axial direction and the small zero point energy $\hbar\omega_\perp$ guarantee that total energy in the short-range three dimensional motion will be small, such that interactions will be s -wave dominated. The resulting 1D scattering lengths are given in equations (12). The very good agreement we obtain between the numerical and the analytical results for both bosons and fermions confirms the physical picture at the basis of (12) and represents a stringent test for our computational approach \ddagger . Note that the condition $\bar{a} \ll a_{ho}$ implies $\alpha^F/\alpha^B = \beta^F/\beta^B \sim (\bar{a}/a_{ho})^4 \ll 1$ in the present case of weak confinement.

Let us now consider the behavior of a_{1D} for nonvanishing d . In the aim of suppressing harmful reactive collisions the molecular dipoles are supposed to be orthogonal to the trap axis and calculations are performed for reference in the zero energy limit. We extract the collision lengths α and β from the numerically calculated a_{1D} using (10). As already remarked below equation (5), the scaling behavior of $\alpha^{B,F}$ can be expected to evolve from the combination of \bar{a} and a_{ho} given by (12) for small dipoles to a_{dd} in the $a_{dd} \gg a_{ho}$ limit. This scaling argument is consistent with the extremely rapid increase of α^F with d from small values $\sim 10^{-3} \bar{a}$ to an approximate scaling with a_{dd} that sets in already for $a_{dd} \approx a_{ho}$. On the converse, the bosonic analogue α^B is initially large ($\alpha^B = 25 a_{ho}$) and *drops* to values on the order of a_{dd} for $a_{dd} \approx a_{ho}$.

\ddagger For a fully quantitative comparison small corrections to (12) of the order \bar{a}/a_{ho} have been taken into account; see equation (3) of (Michele et al. 2010).

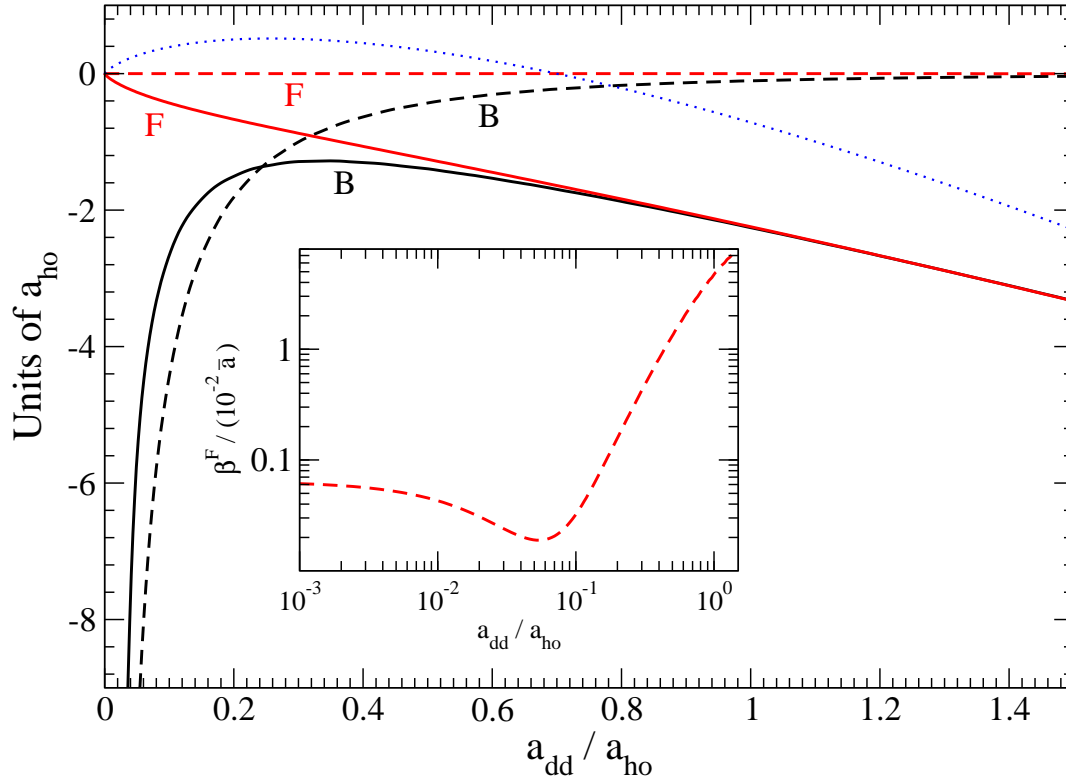


Figure 3. Main panel : the collision lengths α (full lines) and $-\beta$ (dashed lines) defined in equations (4) and (5), calculated numerically in the $E \rightarrow 0$ limit for bosonic (B) and fermionic (F) polar molecules as a function of the dipolar length a_{dd} . Transverse confinement $a_{ho} = 100 \bar{a}$ is weak. The universal dipolar contribution $b_3 \log(q|b_3|)$ is also shown (dotted line) for a collision energy of $E/k_B = 5$ nK and the reduced mass of K-Rb. Inset : enlarged view of β^F in log-log scale. Note the different units used for the vertical axis in the two panels.

Note from (8) that in the $E \rightarrow 0$ limit one simply has $\mathcal{K}^{\text{inel}} \propto \beta$. The behavior of β with d represented in figure 3 can thus be interpreted in terms of the reactive rate, *i.e.* of the flux that reaches the spherical surface of radius a_c and that in our model is fully adsorbed. From this viewpoint, for collisions of bosonic molecules that do not present any barrier at short range the long-range repulsion occurring at perpendicular configuration for $d > 0$ will directly tend to suppress the reaction. More quantitatively, the minimum energy path connects a repulsive and an attractive potential valley crossing a saddle point \bar{r}^* where the net force vanishes. It can be easily found that this point is located in the plane of the dipoles at a distance $r^* = 6^{1/5} a_{ho}^{4/5} a_{dd}^{1/5}$ from the origin with polar angle $\sin^2(\theta^*) = 1/5$. The potential energy barrier at the saddle point is d^2/r^{*2} . Tunneling through the barrier results in the strong decrease of β^B with a_{dd} observed in figure 3.

The reaction dynamics of fermionic molecules is qualitatively different as it is mainly controlled by the short-range potential barrier arising from the combination of the van der Waals attraction and of the centrifugal repulsion illustrated in figure 1. It is the presence of this barrier that results in the suppression of β^F both for vanishing and

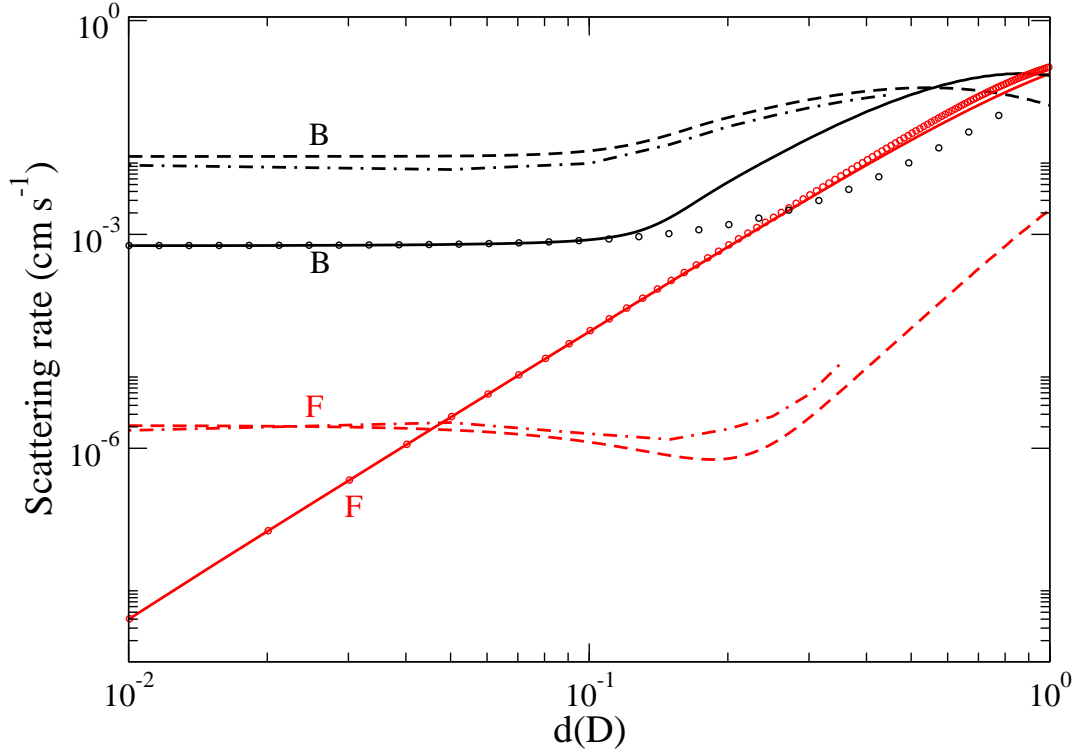


Figure 4. Numerically calculated elastic and inelastic collision rates for polar molecules in quasi-1D geometries as a function of the induced dipole moment at a collision energy $E/k_B = 5$ nK. Transverse confinement $a_{ho} = 100 \bar{a}$ is weak and K-Rb molecular parameters have been used. Elastic (full lines) as well as reactive rates (dashed lines) are shown for bosons (B) and fermions (F). The points indicate the result of distorted wave Born approximation to the elastic collision rates (see text). The dot-dashed lines represent the reactive rates calculated for the lowest adiabatic potential determined by diagonalization of the full matrix potential in the spherical basis (see text for details)

finite d with respect to the barrierless bosonic case; see the inset of figure 3. Note that the weak confinement condition $\bar{a} \ll a_{ho}$ implies that the harmonic potential has negligible influence on the barrier shape and position. It can be easily shown that in the absence of dipolar forces the energetically lowest effective barrier with $\ell = 1$ is located at $r_1 = 2.3153 \bar{a}$.

In a perturbative picture valid for weak dipoles, the $\ell = 1$ barrier is modified by the dipolar interaction by an amount $\delta E = \langle Y_{10} | V_{dd}(r_1) | Y_{10} \rangle_\Omega = d^2/r_1^3$, where the average $\langle \cdot \rangle_\Omega$ is taken on the unit spherical surface. Since $\delta E > 0$, the dipolar force tends to reinforce the barrier thus reducing the reactive rate, *i.e.* β . In other terms, Fermi symmetrization prevents the molecules from occupying the regions near the $z = 0$ plane where the head-to-tail attraction is stronger. This perturbative picture begins to fail when $\delta E \sim \hbar^2/(2\mu r_1^2)$ and the repulsion between the fundamental and the excited effective potentials lowers the potential barrier. In this situation the dipolar force becomes dominant over the centrifugal interaction allowing the molecules to tunnel more efficiently through the centrifugal barrier, leading thus to an increased β . The

combination of these large and small d effects accounts for the minimum in β observed for $a_{\text{dd}} \sim \bar{a}$ in figure 3 and is confirmed by the behavior of the adiabatic barriers illustrated in figures 1 and 2.

Note in figure 3 that for $a_{\text{dd}} \gtrsim a_{\text{ho}}$ one has $\beta^{\text{B,F}} \ll \alpha^{\text{B,F}} \sim a_{\text{dd}}$ and to a good approximation $\alpha^{\text{B}} = \alpha^{\text{F}}$. That is, for large dipoles scattering is mainly elastic and the elastic scattering phases of boson and fermions are very similar since they are accumulated at long range where the effect of bosonic/fermionic statistics is immaterial. We will come back in some more detail on such boson-fermion equivalence in the following.

Let us now model more realistic experimental conditions in a finite temperature gas. To this aim the collision energy will be fixed at a small yet finite value $E/k_B = 5$ nK, which for K-Rb molecules is below the trap level spacing $2\hbar\omega_{\perp}$; see table 1. At these extreme yet experimentally attainable temperatures inelastic transitions $|00\rangle \rightarrow |n'_r\Lambda'\rangle$ with $E_{n'_r\Lambda'} > E_{00}$ are energetically forbidden. Figure 4 shows that the elastic rate for bosons presents a relatively weak dependence on d with an overall variation of about one order of magnitude for d below 1 D. Let us remark that the general structure of (6) predicts no dependence of \mathcal{K}_{el} on d to the extent that $(\alpha q)^2, \alpha b_3 q^2, (\beta q) \ll 1$. The variation of \mathcal{K}_{el} with d and in particular the broad maximum observed for $a_{\text{dd}} \sim q^{-1}$ results therefore from energy-dependent terms in the denominator of (6), which are non-negligible even at our small collision energy.

The elastic rate in the case of fermionic molecules presents on the converse a dramatically rapid increase. In fact, generalizing the arguments invoked for $E \rightarrow 0$ to finite energy, the dipolar length a_{dd} rapidly overcomes \bar{a} in setting the scale of a_{1D} and thus of \mathcal{K} through (7). On a more quantitative ground, DWBA accurately describes the elastic collision rate for fermions in the investigated range of dipole moments, while for bosons higher order terms can play an important role and the DWBA is not as accurate.

The reactive rate for bosons represented in figure 4 can be partly understood based on the zero-energy limit results, which show a monotonically decreasing β . In fact, since we numerically obtain a similar monotonic behavior also for the finite energy quantity $\beta(q)$ and at our collision energy $q\beta \sim 1$ the maximum is once again due to finite-energy corrections in the denominator of (8). This kind of behavior was also predicted for quasi-2D dipolar collisions (Julienne et al. 2011) and can intuitively be explained by the shape of the interaction potential. Since repulsion affects more strongly slower collisions the drop of $\mathcal{K}^{\text{inel}}$ with d and hence the location of the maximum shifts at smaller d for decreasing E . Note that in the present weak confinement geometry the reactive rate of bosonic molecules varies relatively little, less than one order of magnitude for $d < 1$ D, and that the ratio of elastic to inelastic collision is of order one and thus not favorable for experiments where a long lifetime is needed.

To conclude, the inelastic rate for fermions in figure 4 presents a modulation that closely mirrors the behavior of the zero-energy inelastic length β^{F} in figure 3. That is, finite-energy corrections do not modify the reaction barrier arguments used for $E \rightarrow 0$. Such arguments can then be repeated in the present case to explain the presence of the

shallow minimum for $d \approx 0.2$ D. The ratio of inelastic to elastic collision rates becomes very favorable for moderate dipole moments $d \sim 0.1$ D. We have also checked that as expected the fermionic reactive rate does not grow indefinitely with d since the long-range repulsion between dipoles perpendicular to the trap will affect fermion dynamics on the same footing as it does for bosons.

2.2. Intermediate confinement

We now consider a case with stronger yet experimentally realizable confinement; $a_{\text{ho}} = 10 \bar{a}$. As expected, we find that the $d = 0$, $E \rightarrow 0$ closed expressions (12) valid for $\bar{a} \ll a_{\text{ho}}$ do not predict correctly the elastic collision length α , which depends on the detailed long-range interplay of trapping and van der Waals potentials. However, the analytical result is still surprisingly accurate for estimating the inelastic length β , which is a coarser quantity proportional to the overall flux reaching the adsorbing boundary. Therefore, from (8) one finds that $\mathcal{K}^{\text{inel}}(q \rightarrow 0) \propto \beta$ decreases for bosons as a_{ho}^{-2} whereas it increases for fermions with a_{ho}^2 . As far as it concerns elastic scattering, taking the

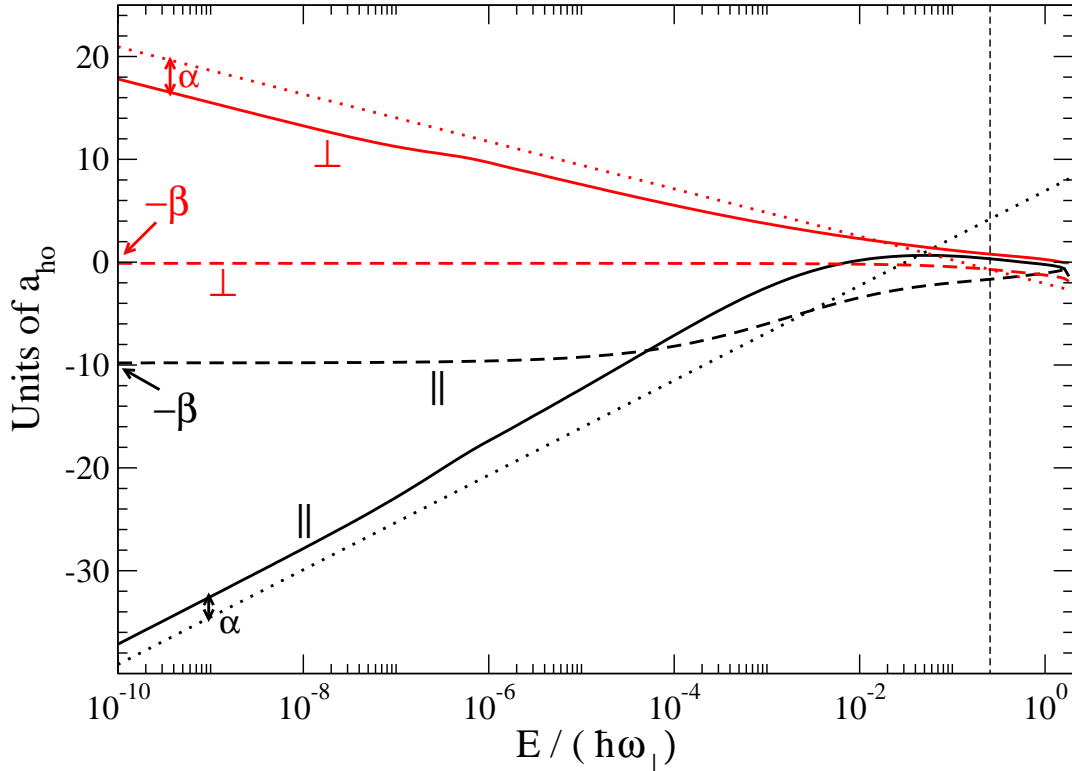


Figure 5. Real (full lines) and imaginary (dashed lines) parts of the 1D scattering length as a function of collision energy for a dipole moment such that $a_{\text{dd}} = a_{\text{ho}}$ in the case of intermediate confinement $a_{\text{ho}} = 10 \bar{a}$. Results are for bosonic molecules with dipole oriented orthogonal \perp or parallel \parallel to the trap axis. The dotted lines represent the universal term $b_3 \log(b_3|q|)$. The zero-energy limit of the elastic and inelastic collision lengths α and β is shown by arrows. The vertical line indicates a realistic experimental temperature of 500 μK .

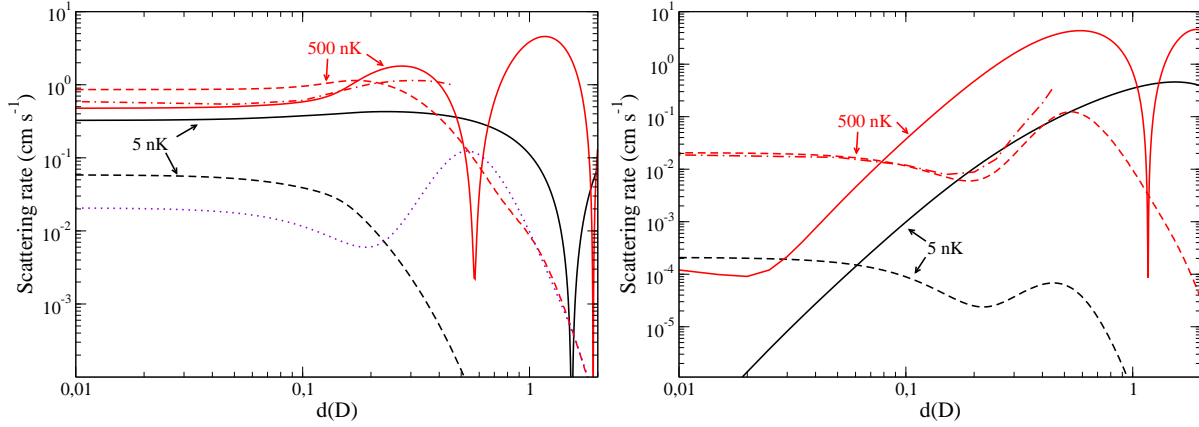


Figure 6. Numerically calculated elastic and inelastic collision rates for polar molecules in quasi-1D geometries as a function of the induced dipole moment for intermediate transverse confinement $a_{ho} = 10\bar{a}$. Full (dashed) lines in the leftmost panel represent the elastic (inelastic) collision rates at energy $E/k_B = 5$ and 500 nK for bosonic molecules. The rightmost panel shows the analogous quantities for collisions of fermionic molecules. The dot-dashed lines on both panels show the results of the adiabatic approximation for $E/k_B = 500$ nK. The fermionic inelastic rate at energy $E/k_B = 500$ nK has been included for comparison in the leftmost panel (dotted line).

$q \rightarrow 0$ limit of (6,7) one finds that the \mathcal{K}_{el} only depends on the dipolar strength b_3 through the logarithmic universal term, independent of confinement. However, as in weak confinement such zero-energy limit behavior is essentially formal as it only holds at extremely low energies.

Examples for a finite dipole moment oriented parallel and perpendicular to the trap axis are reported in figure 5. One can verify that the Wigner regime is correctly reproduced by the numerical calculation for both molecular orientations but is attained below $10^{-7} \hbar\omega_{\perp}$ ($10^{-4} \hbar\omega_{\perp}$) for the elastic (inelastic) collision lengths. It is also interesting to observe that at parallel polarization β , in addition to α , has a relatively large value of order a_{dd} . It is important to remark that even at parallel configuration, in spite of the attractive character of the long-range interaction the reaction rate does not reach the unitarity limit at low collision energy. This is easily seen by observing that the reaction probability is simply the reactive rate normalized to the relative velocity v , and that the former quantity reduces to $4q\beta$ for $q \rightarrow 0$. The reaction probability therefore vanishes with collision energy due to the complete reflection of the incoming flux on the *attractive* long-range potential tail, a purely quantum effect known as quantum reflection. This phenomenon quantifies the deviation of the quantum dynamics from the semiclassical limit and is known to be supported by inverse-cubic potentials (Côté et al. 1997).

Once again, such complete quantum reflection only takes place at extremely small collision energy, and finite energy calculations are necessary to predict collisions rates even at the characteristic temperatures of an ultracold gas. For instance, figure 6 summarizes our findings at 5 nK. The $d = 0$ reactive rate for bosons in intermediate

confinement is about 5 times larger than the corresponding weak confinement value, in contrast with the $E \rightarrow 0$ scaling with a_{ho}^{-2} observed above. The fermionic $d = 0$ reactive rate for intermediate confinement about 10^2 times larger than the corresponding weak confinement value, in good agreement with the a_{ho}^2 zero-energy law. As in the weak confinement case, a maximum in $\mathcal{K}_{\text{el}}^{\text{B}}$ is observed as a function of d , followed by a pronounced Ramsauer-Townsend minimum where the elastic collision rate drops to extremely small, yet nonzero, values. The Ramsauer minimum shifts at smaller d for increasing collision energy. A similar behavior is observed for $\mathcal{K}_{\text{el}}^{\text{F}}$.

The reactive rates show a qualitatively similar behavior as in weak confinement, comprising a maximum for bosons, and a minimum followed by a maximum for fermions. These results qualitatively agree with the behavior of adiabatic barrier heights. However, due to the smaller oscillator length here one gets more deeply in the regime $a_{\text{dd}} > a_{\text{ho}}$ where the reactive rates are strongly suppressed. In fact, in simple terms a tighter transverse trap prevents more efficiently the molecules from approaching along attractive head-to-tail reaction paths. The suppression with d becomes exponential for $a_{\text{dd}} \gg a_{\text{ho}}$ as implied by semiclassical tunneling through the potential energy barrier about the transition saddle point r^* . We conclude that increasing the confinement is advantageous for reaching a favorable rate of elastic and inelastic collision rates, or a slow inelastic rate *tout court*. One may work for instance in the minimum region of $\mathcal{K}^{\text{inel}}$ for fermionic K-Rb, or simply increase d to large values, which is possible for more polar bosonic or fermionic species such as Li-Cs. Unfortunately, the present results also show that in the case of bosonic K-Rb, for which realistic induced dipole moments are below 0.3 D, a significant suppression of $\mathcal{K}^{\text{inel}}$ can only be attained at low temperatures of the order of few nK.

It is interesting to remark in the leftmost panel of figure 4 that in the limit of large d the reactive rates for fermions and bosons tend to coincide. The numerical calculation shows indeed not only the approximate identity of the rates but the stronger condition on the scattering matrices $S^{\text{B}} = -S^{\text{F}}$. This form of universality, often termed boson fermionization, can be qualitatively understood as follows. The boundary condition set on the inner sphere is universal since it completely adsorbs all flux reaching short range irrespective of the bosonic or fermionic nature of the colliding particles. The dynamics at sufficiently long range $r \gg a_{\text{ho}}$ is also universal because particle statistics does not play any role in this region. Departures from universality arise in the transition from long to the short range. That is, potential barrier or quantum reflection may prevent part of the flux of the incoming wave from reaching the inner adsorbing boundary. As the dipole increases ($a_{\text{dd}} > a_{\text{ho}}$), motion driven by the dipolar interaction tends to become semiclassical and quantum reflection is suppressed. Hence, also wave transmission inside the sphere of radius $r \approx r^*$ will not depend on quantum statistics. Note, however, that this does not mean that the rate reaches the unitarity limit since the incoming wave is reflected by the dipolar potential at internuclear distances $r \gtrsim r^*$. We can equivalently state that universality arises when the transition saddle points resides in a region where molecule exchange is irrelevant, *i.e.* when $r^* \gg a_{\text{ho}}$. Keeping into account the

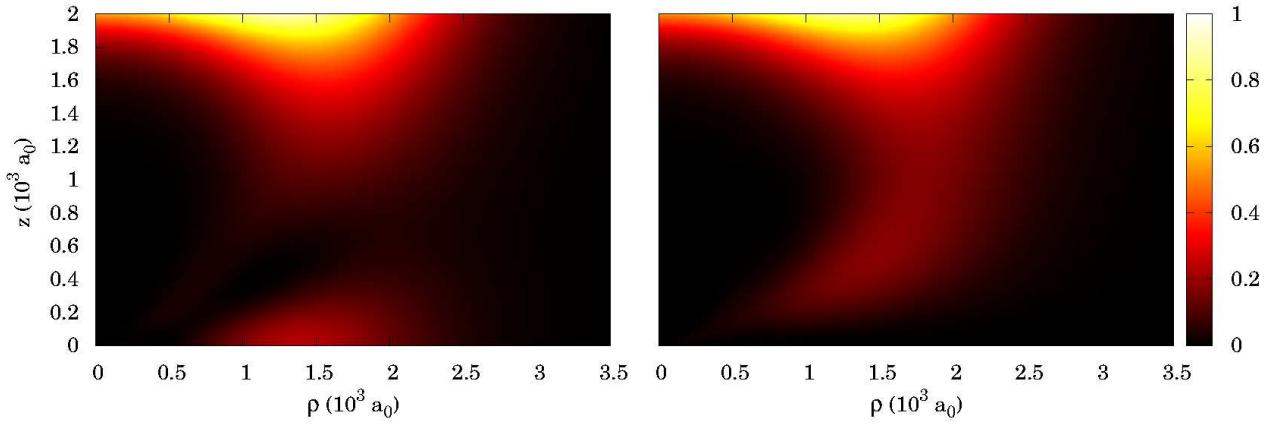


Figure 7. Radial probability density $r^2|\psi(\vec{r})|^2$ (in arbitrary units) for collisions of bosonic (right panel) and fermionic (left panel) K-Rb polar molecules in the plane containing the trap z axis and the molecular dipoles in the case of intermediate confinement. Collision energy is low $E/k_B = 5$ nK and the dipole is sufficiently strong $d = 1$ D ($a_{dd} \simeq 15 a_{ho}$) to be in the boson fermionization regime (see text).

asymptotic form (3) of the wavefunction one can conclude that fermionization $S^B = -S^F$ results from the combination of the argument above *and* of the different sign convention for the bosonic/fermionic asymptotic wavefunction. Of course the elastic rates, while related through the relation $|1 - S_{jj}^B|^2 = |1 + S_{jj}^F|^2$, do differ in general.

It should be stressed that universality only concerns asymptotic properties and does not imply similar dynamical behavior for bosons and fermions at short distances. Figure 7 shows for instance the molecule probability density in the plane of the dipoles for $r \lesssim a_{ho}$ and $d = 1$ D, where one can clearly observe different patterns for bosons and fermions with in particular the effect of particle symmetrization making the fermionic wavefunction vanish in the $z = 0$ plane. One may also notice that the strong repulsion between parallel dipoles pulls the molecules away from the trap axis.

Full three dimensional analysis is represented in figure 8 in the case of bosonic molecules, where by symmetry we considered the $z > 0$ half space only. One clearly observes that for decreasing distance the probability distribution becomes quite strongly confined by dipolar repulsion in the plane containing the dipoles and the trap axis (plane xz), with a vanishingly small amplitude in the yz plane. Interestingly, one may remark the presence of a relatively large closed line (a smoke ring) where the density probability vanishes. Inspection of the velocity field shows that the streamlines encircle the nodal ring, a configuration termed toroidal vortex in the seminal paper of (Hirschfelder et al. 1976). It is worth stressing that the presence of the vortex is not due to a singularity in the potential but merely to quantum interference effects. The presence of vortices has also been observed in the context of one dimensional quantum reactive models (Hirschfelder 1976), although in the present case of ultracold energies

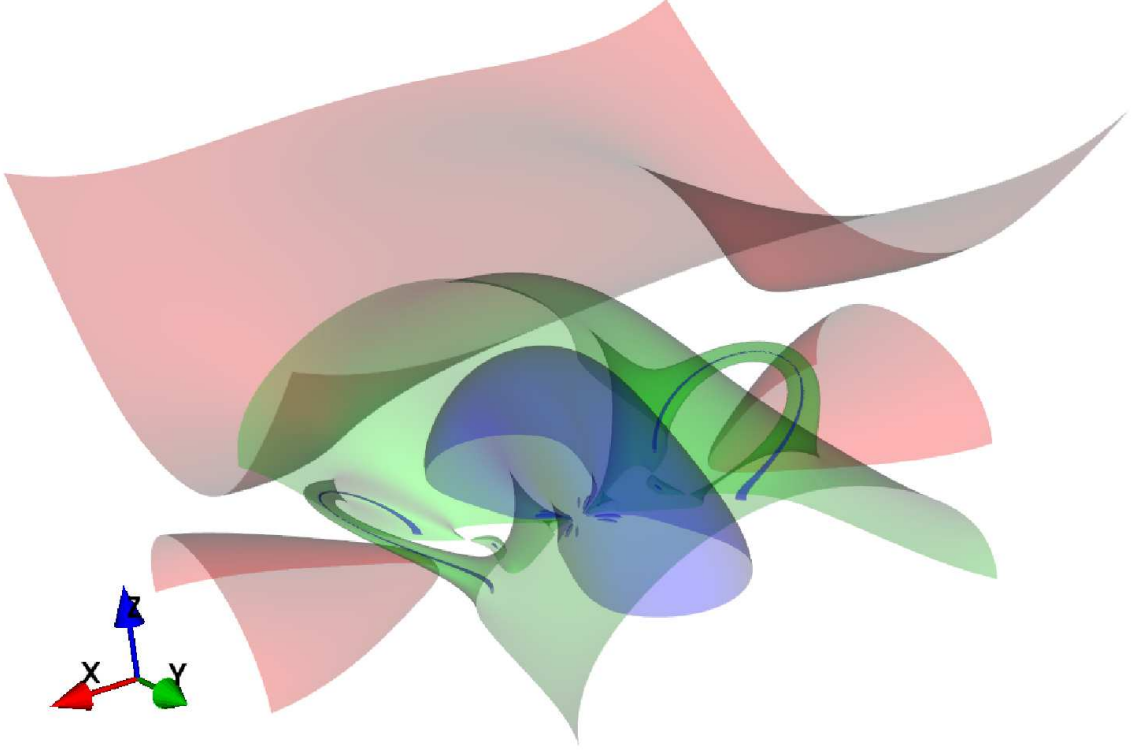


Figure 8. Isosurfaces of the probability density for the scattering bosonic wavefunction. The quantity $r^2|\psi(\vec{r})|^2$ is constant on each surface and varies by two order of magnitudes from one surface to the other, increasing from colder to warmer color codes. The wavefunction is represented in a three dimensional box of equal $1750 a_0$ sides. The isosurfaces are symmetric with respect to the xz and yz planes. Physical parameters are as in figure 7.

the size the rings are localized to larger distances (larger than about $3\bar{a}$ in the case of the figure, in a region dominated by dipolar forces). We observe the presence of a similar toroidal vortex in the fermionic case as well (not shown) with the notable difference that the vortex now crosses the nodal $z = 0$ plane in two exceptional points.

To conclude, it is interesting to compare the efficiency of suppressing reactive collisions using quasi-1D and quasi-2D confinement. We consider both the ratio between reactive and elastic collisions and the effective decay rate $\Gamma = \mathcal{K}^{\text{react}} n$, where n is the d -dimensional number density measured in cm^{-d} , which can be transformed to equivalent 3D density via $n_{3D} = n/a_{ho}^{3-d}$. In a pancake-shaped trap with dipoles aligned to repel each other, significant suppression of reaction rates has been reported (Micheli et al. 2010, Quémener & Bohn 2011, Julienne et al. 2011). Here, we find that confining the system in additional direction does not lead to significant improvements. Figure 9 shows indeed our results for $a_{ho} = 10 \bar{a}$ at $E/k_B = 500\text{nK}$ for bosons and fermions.

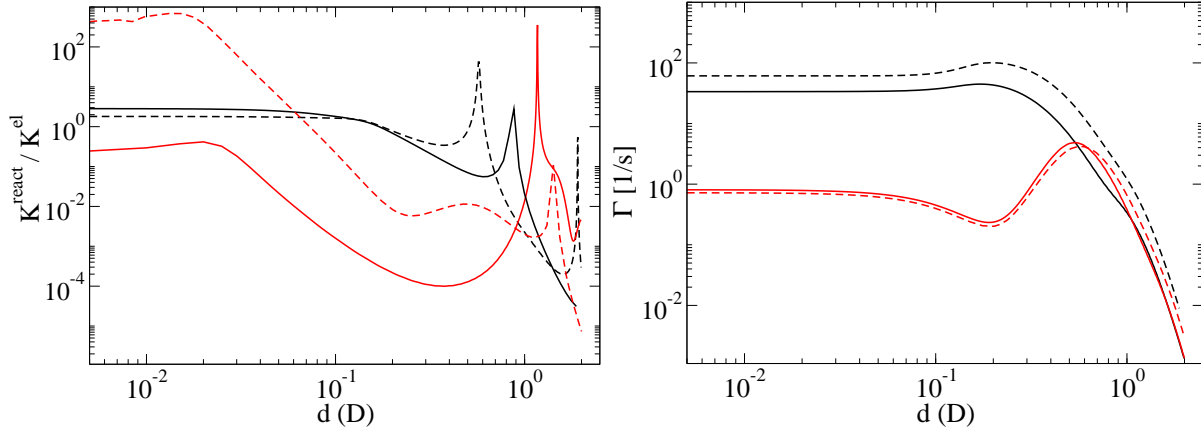


Figure 9. Left: the ratio between reactive and elastic collision rates for bosons (black) and fermions (red) confined in quasi-1D (full lines) or quasi-2D (dashed lines) trap with $a_{ho} = 10 \bar{a}$ at collision energy $E/k_B = 500\text{nK}$. Right: the decay rates $\Gamma = \mathcal{K}^{\text{react}} n$ for the same parameters and equivalent 3D density equal to 10^{12}cm^{-3} .

In the case of bosons, both the ratio between reactive and elastic collision rates and the decay rate are similar for 1D and 2D. For fermions we find some improvement in the ratio in one-dimensional setups. However, comparing only the rate constants does not include the impact of many-body correlations, which induce strong suppression of reactions in one dimension via continuous Zeno effect (Zhu et al. 2014), especially when a lattice potential is present along the tube direction.

2.3. Strong confinement

In the strong confinement case $a_{ho} = \bar{a}$ the trap is so tight that its effect becomes important even on the short scale of the van der Waals interaction. As shown on figure 10, the elastic rates for bosons and fermions initially differ by more than one order of magnitude for $d = 0$ and become soon comparable as a function of d , with the bosonic curve showing a pronounced Ramsauer-Townsend minimum.

Quite strikingly the reactive rates for bosons and fermions are quantitatively very similar even for $d = 0$, and become exponentially suppressed with d . As in the case of intermediate confinement, the numerical calculation shows that to very good accuracy $S^B = -S^F$. Moreover, wavefunction inspection (not shown) reveals that the density probability amplitudes are very similar for bosons and fermions at all distances, with minor differences only at $r \approx r_c$. In simple terms we can summarize by saying that confinement is so strong that it effectively prevents molecule exchange and under these conditions the particle statistics becomes immaterial both with respect to the elastic and the inelastic dynamics. The system behaves therefore as a truly 1D (as opposed to quasi-1D) system.

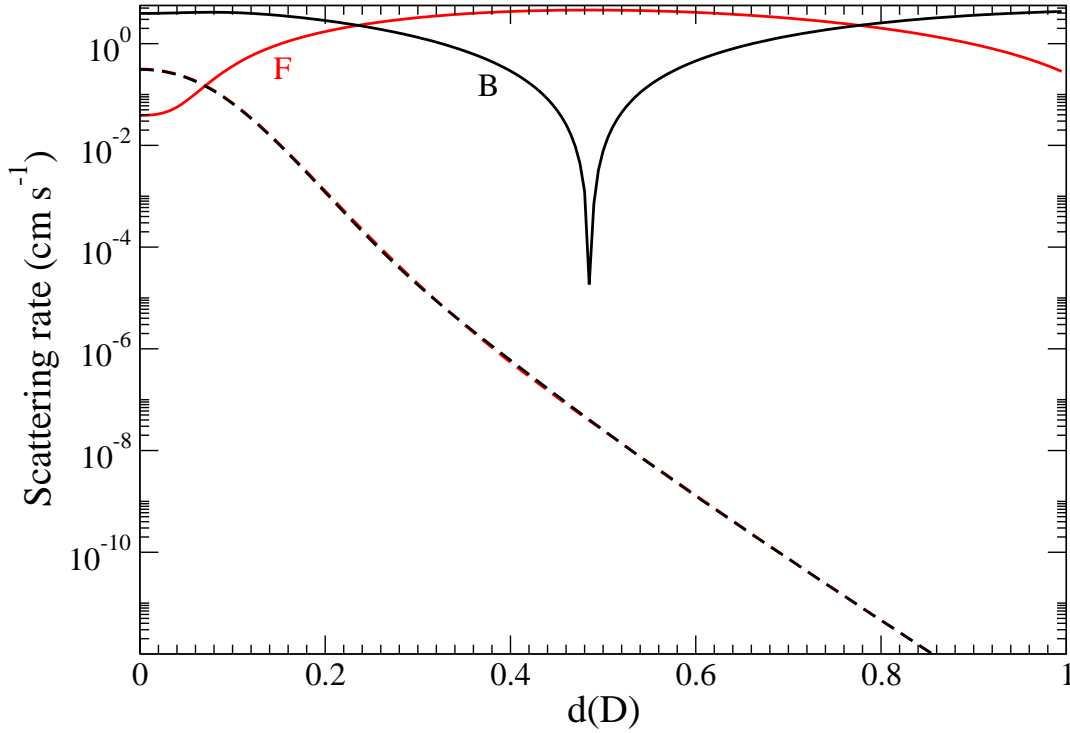


Figure 10. Same as figure 4 but for strong confinement and $E/k_B = 500$ nK.

2.4. Inelastic collisions (intermediate confinement)

If the molecules are not prepared in the ground state of the transverse oscillator, inelastic transitions to lower trap levels can occur even at very low collision energy. We show as an example in figure 11 the low energy collision rates for bosonic molecules prepared in either degenerate initial states $|10\rangle$ or $|02\rangle$.

As a general feature, collisions starting with molecules with a relative axial angular momentum $\Lambda > 0$ experience a centrifugal barrier in the incoming channels that pushes the molecules away from the trap axis hence suppressing the collisional interaction. Such effect is observed both for elastic and reactive processes, and is very pronounced for the inelastic $|02\rangle \rightarrow |10\rangle$ process. Molecule preparation in a quantum state with $\Lambda > 0$ is therefore at least in principle a mean to control inelastic and reactive collision rates.

It is interesting to observe in figure 11 that as the dipole moment increases above $d \approx 0.3$ D, the dipolar force dominates the centrifugal barrier at long range, giving rise to a novel universal behavior in which the elastic $|n_r\Lambda\rangle \rightarrow |n_r\Lambda\rangle$ collision rates become independent of the initial quantum numbers. Inelastic transitions between trap levels are found to proceed at comparable rates as the reactive ones, both being progressively suppressed with d . Finally, superelastic (energetically neutral) $|10\rangle \leftrightarrow |02\rangle$ collision tend to be slow at each d .

The fermionic case summarized in figure 12 shares with the bosonic case some qualitative features such as the drop of the inelastic and reactive rates for large d . However, fermionic symmetry implies the presence of a centrifugal barrier even for an

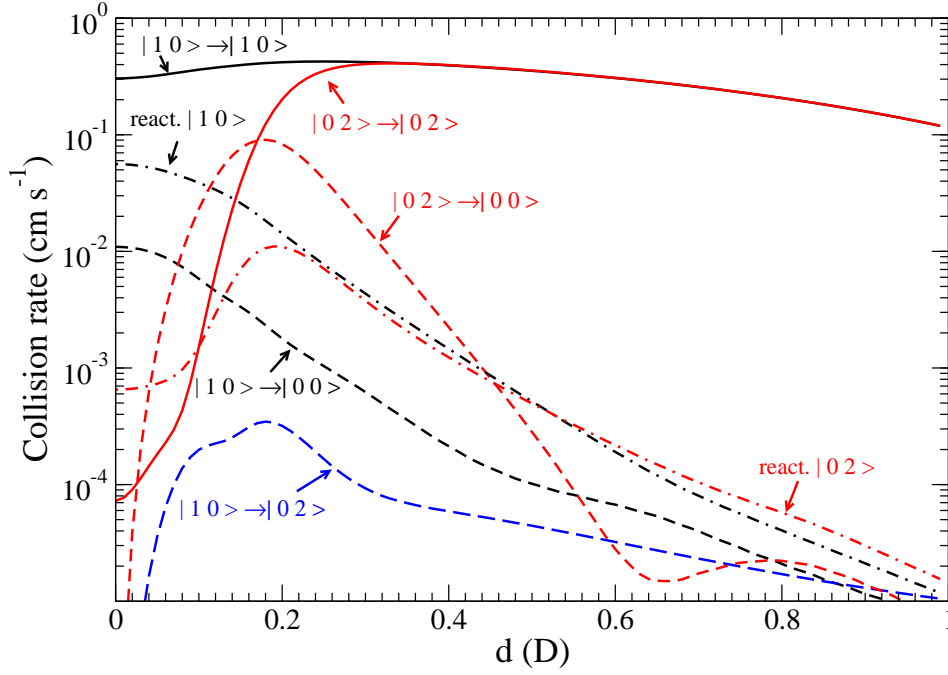


Figure 11. Elastic (full lines), superelastic (long-dashed line), inelastic (short-dashed lines), and reactive (dash-dotted lines) collision rates for bosonic molecules in a 1D-trap as a function of the molecular dipole moment. Different state-to-state $|n_r\Lambda\rangle \rightarrow |n'_r\Lambda'\rangle$ processes are separately shown for $|10\rangle$ and $|02\rangle$ initial states. Results are for intermediate confinement and fixed collision energy $E/k_B = 5$ nK. Calculation is performed for a Hamiltonian symmetry block $\{\pi_x, \pi_y\} = \{1, 1\}$ containing the ground state of the transverse oscillator.

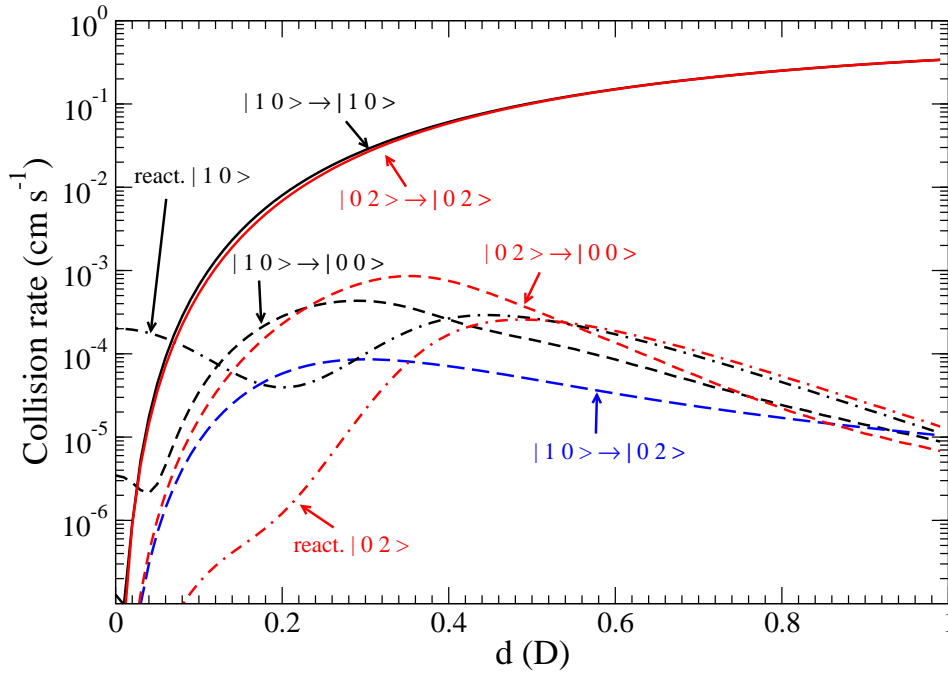


Figure 12. Same as figure 11 but for fermions.

initial $\Lambda = 0$, such that the elastic $|10\rangle \rightarrow |10\rangle$ collision rate section is also strongly suppressed and follows in fact very closely the evolution of the $|02\rangle \rightarrow |02\rangle$ curve with d . The reactive and inelastic rate are on the converse several orders of magnitudes smaller for collisions starting in $|02\rangle$ than in the $|10\rangle$ quantum state, because of the presence of a stronger effective barrier mainly determined by the $\ell = 3$ partial wave rather than 1 as in the case of $|10\rangle$ collisions.

2.5. Dependence on the molecular dipole orientation (intermediate confinement)

Varying the orientation of the molecular electric dipoles can provide another knob to control the collision dynamics in the experiments. We represent in figure 13 the collision rates at two sample collision energies $E/k_b = 5$ and 500 nK for bosonic and fermionic molecules for a dipole moment such that $a_{dd} = a_{ho}$ (see table 1 for typical numerical values) in an intermediate confinement geometry. In order to ease the comparison

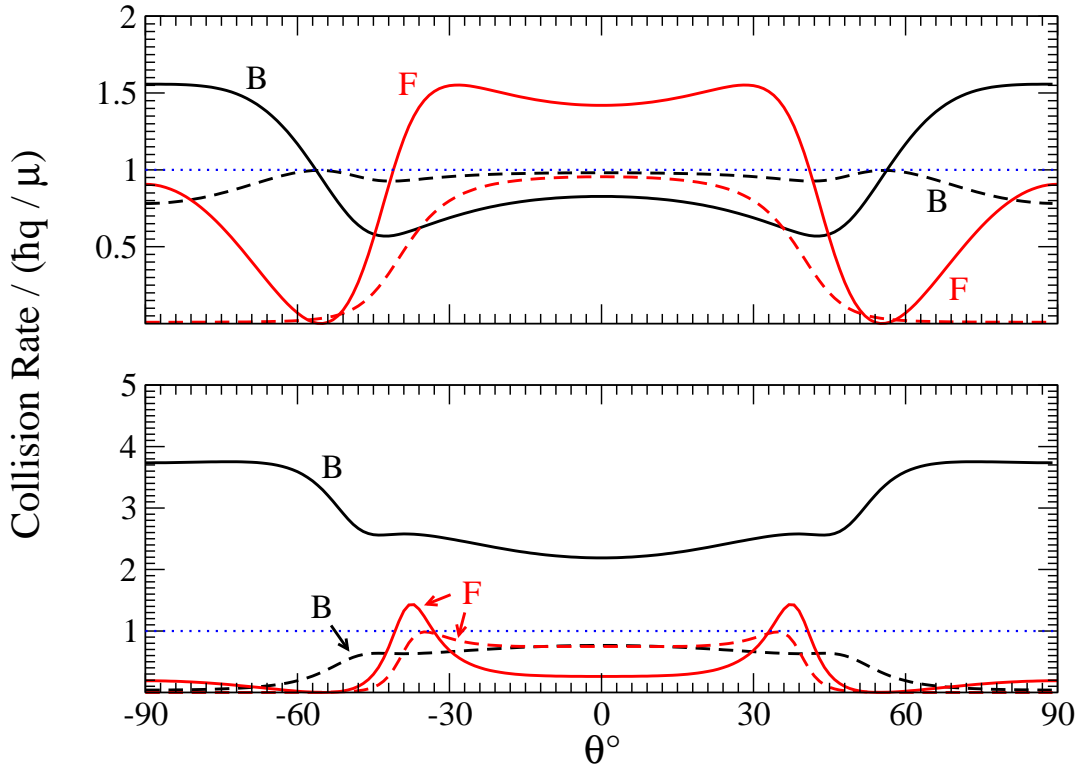


Figure 13. Collision rates as a function of the polar angle θ between \vec{d} and the trap axis z . Elastic (full lines) and inelastic (dashed lines) rates normalized to the relative velocity are shown for bosons (B) and fermions (F) at a collision energy of $E/k_B = 5$ nK (lower panel) and 500 nK (upper panel). The dotted lines represent the upper limit of the reactive collision rates.

reactive collision rates reach their minimum value when the molecular dipoles are in a repulsive configuration orthogonal to the trap axis. The maximum takes place at parallel

configuration, where boson and fermions react at a common rate. The lower panel of figure 13 demonstrates that at 5 nK the rate is still relatively far from the unitarity limit $\mathcal{K}^{\text{react}} = \hbar q/\mu$, meaning that quantum reflection is significant. Conversely, at 500 nK (upper panel in figure 13) the reactive rate is close to unitarity.

One may also note that the elastic rate for fermions is strongly suppressed at a specific (magic) value of the angle, which is in a good approximation given by the condition $b_3 = 0$, corresponding to $\theta \approx 55^\circ$. Since this value is robust against changes in the collision energy, a non-interacting gas behavior should be experimentally observable in a thermal sample by a suitable choice of the direction of the polarizing electric field. Finally, the elastic rate for bosons is modulated as a function of the dipole orientation but its overall range of variation and hence the possibility of experimental control is relatively limited at both investigated temperatures.

3. Conclusions

In conclusion, we have theoretically studied polar molecule collisions in quasi-1D geometries. Our numerical model allows us to treat dipole strengths of experimental interest for dipoles forming an arbitrary angle with the trap axis. As expected, polarizing the molecular electric dipoles orthogonal to the trap axis allows one to suppress undesired reactive rates by increasing the magnitude of d . Unfortunately, for moderate dipole moments of commonly used species such as bosonic K-Rb such suppression is only significant at very low temperatures or extremely tight confinement. We have identified a dipolar universal regime where bosons and fermions present equivalent asymptotic behavior at large r or, in the case of extremely tight confinement, equivalent dynamical behavior at all distances. We also showed that in terms of suppressing the reactive collisions, quasi-1D confinement gives little advantage over the quasi-2D one.

In the case where the molecules populate excited trap states, inelastic processes have been found to proceed essentially at a similar rate as the reaction. The influence of the molecular dipole orientation on collision is quantitatively important in particular for elastic scattering of fermionic molecules, that become non-interacting at a magic value of the dipole-trap axis angle.

In perspective, it may be interesting to apply the model introduced here to non-reactive species and to extend our calculations to larger values of d by relaxing the fixed-dipole approximation.

Acknowledgments

We would like to thank G. Modugno for useful discussions. This work was supported by the Agence Nationale de la Recherche (Contract No. ANR-12-BS04-0020-01), Foundation for Polish Science International PhD Project co-financed by the EU European Regional Development Fund and National Center for Science grants DEC-2011/01/B/ST2/02030 and DEC-2013/09/N/ST2/0218.

References

- Bartolo N, Papoular D J, Barbiero L, Menotti C & Recati A 2013 *Phys. Rev. A* **88**, 023603.
- Bolda E L, Tiesinga E & Julienne P S 2002 *Phys. Rev. A* **66**, 013403–1–7.
- Capogrosso-Sansone B, Trefzger C, Lewenstein M, Zoller P & Pupillo G 2010 *Phys. Rev. Lett.* **104**, 125301–1–4.
- Carr L D, DeMille D, Krems R V & Ye J 2009 *New Jour. Phys.* **11**, 055409–1–87.
- Chotia A, Neyenhuis B, Moses S A, Yan B, Covey J P, Foss-Feig M, Rey A M, Jin D S & Ye J 2012 *Phys. Rev. Lett.* **108**, 080405–1–4.
- Côté R, Friedrich H & Trost J 1997 *Phys. Rev. A* **56**, 1781–1787.
- de Miranda M H G, Chotia A, Neyenhuis B, Wang D, Quémener G, Ospelkaus S, Bohn J L, Ye J & Jin D S 2011 *Nature Physics* **7**, 502–507.
- Delves L M 1960 *Nucl. Phys.* **20**, 275–308.
- Gao B 1999 *Phys. Rev. A* **59**, 2778–2786.
- Giannakeas P, Melezhik V S & Schmelcher P 2013 *Phys. Rev. Lett.* **111**, 183201–1–4.
- Góral K, Santos L & Lewenstein M 2002 *Phys. Rev. Lett.* **88**, 170406–1–4.
- Gorshkov A V, Manmana S R, Chen G, Ye J, Demler E, Lukin M D & Rey A M 2011 *Phys. Rev. Lett.* **107**, 115301.
- Gribakin G F & Flambaum V V 1993 *Phys. Rev. A* **48**, 546–553.
- Hirschfelder J O 1976 in B Pullman & R Parr, eds, ‘The New World of Quantum Chemistry’ Vol. 2 of *Académie Internationale Des Sciences Moléculaires Quantiques / International Academy of Quantum Molecular Science* Springer Netherlands pp. 81–86.
- Hirschfelder J O, Goebel C J & Bruch L W 1976 *J. Chem. Phys.* **61**, 5456–5459.
- Idziaszek Z & Julienne P S 2010 *Phys. Rev. Lett.* **104**, 113202–1–4.
- Jachymski K, Krych M, Julienne P S & Idziaszek Z 2013 *Phys. Rev. Lett.* **110**, 213202.
- Julienne P S, Hanna T M & Idziaszek Z 2011 *Phys. Chem. Chem. Phys.* **13**, 19114–19124.
- Kotochigova S 2010 *New Jour. Phys.* **12**, 073041–1–16.
- Krems R 2008 *Phys. Chem. Chem. Phys.* **10**, 4079–4092.
- Lepetit B, Launay J M & Le Dourneuf M 1986 *Chem. Phys.* **106**, 103–110.
- Micheli A, Idziaszek Z, Pupillo G, Baranov M A, Zoller P & Julienne P S 2010 *Phys. Rev. Lett.* **105**, 073202–1–5.
- Muller T O 2013 *Phys. Rev. Lett.* **110**, 260401–1–5.
- Naidon P & Julienne P S 2006 *Phys. Rev. A* **74**, 062713.
- Ni K K, Ospelkaus S, Wang D, Quémener G, Neyenhuis B, de Miranda M H G, Bohn J L, Ye J & Jin D S 2010 *Nature* **464**, 1324–1328.
- Olshanii M 1998 *Phys. Rev. Lett.* **81**, 938–941.
- Ospelkaus S, Ni K K, Wang D, de Miranda M H G, Neyenhuis B, Quémener G, Julienne P S, Bohn J L, Jin D S & Ye J 2010 *Science* **327**, 853–857.
- Quémener G & Bohn J L 2010a *Phys. Rev. A* **81**, 060701(R).
- Quémener G & Bohn J L 2010b *Phys. Rev. A* **81**, 022702–1–9.
- Quémener G & Bohn J L 2011 *Phys. Rev. A* **83**, 012705.
- Quemener G & Julienne P S 2012 *Chem. Rev.* **112**, 4949–5011.
- Rawitscher G H, Esry B D, E.Tiesinga, Jr. J B & Koltracht I 1999 *J. Chem. Phys.* **111**, 10418–10426.
- Sadeghpour H, Bohn J, Cavagnero M, Esry B, Fabrikant I, Macek J & Rau A 2000 *Journal of Physics B: Atomic, Molecular and Optical Physics* **33**, R93.
- Simoni A & Launay J M 2011 *J. Phys. B* **44**, 235201.
- Sinha S & Santos L 2007 *Phys. Rev. Lett.* **99**, 140406.
- Sowiński T, Dutta O, Hauke P, Tagliacozzo L & Lewenstein M 2012 *Phys. Rev. Lett.* **108**, 115301.
- Syassen N, Bauer D, Lettner M, Volz T, Dietze D, Garcia-Ripoll J, Cirac J, Rempe G & Dürr S 2008 *Science* **320**, 1329–1331.
- Wall M & Carr L 2010 *Phys. Rev. A* **82**, 013611.

Yi S, Li T & Sun C P 2007 *Phys. Rev. Lett.* **98**, 260405–1–4.

Zhu B, Gadway B, Foss-Feig M, Schachenmayer J, Wall M, Hazzard K, Yan B, Moses S, Covey J, Jin D, Ye J, Holland M & Rey A 2014 *Phys. Rev. Lett.* **112**, 070404–1–4.

Żuchowski P S, Kosicki M, , Kodrycka M & Soldán P 2013 *Phys. Rev. A* **87**, 022706.